Supplemental Material for

"Genome-resolved metagenomic analysis reveals different functional potentials of multiple *Candidatus* Brocadia species in a full-scale swine wastewater treatment system"

Yabing Meng[a,b,c], Depeng Wang[a,b,c*], Zhong Yu[a,b,c], Qingyun Yan[a,b,d], Zhili He[a,b,d] and Fangang Meng [a,b,c*]

[a] School of Environmental Science and Engineering, Sun Yat-sen University, Guangzhou 510275, China

[b] Guangdong Provincial Key Laboratory of Environmental Pollution Control and Remediation Technology (Sun Yat-sen University), Guangzhou 510275, China

[c] National Engineering Laboratory for Pollution Control and Waste Utilization in Livestock and Poultry Production, Changsha, 410125, China

[d] Southern Marine Science and Engineering Guangdong Laboratory (Zhuhai), Zhuhai, 519082, China

*** Corresponding author**

Depeng Wang, Ph.D. Email: wangdp6@mail.sysu.edu.cn

Fangang Meng, Ph.D., Email: mengfg@mail.sysu.edu.cn

Contents

Fig. S2 Concentrations of nitrogen (a) and organic matter (b) and the pH, dissolved oxygen, and temperature (c) in different tanks of the full-scale swine wastewater treatment plant.

Fig. S3 Photos of the floc and granular sludge.

Fig. S4 The analysis pipeline for metabolic versatility in this study, including (1) the approaches to reconstruct genome bins, (2) the approaches to infer metabolisms of genomes.

Fig. S5 Microbial community composition of the major phyla (a) and genus (b) in the anammox consortia according to the contig analysis.

Fig. S6 (a) Total abundance of nitrogen metabolic genes. (b) Reconstructed nitrogen metabolic network. (c) Total abundance of nitrogen metabolic processes in different anammox consortia and microorganisms.

Fig. S7 Position SW510 (a) and SW773 (b) on neighbor-joining 16S rRNA gene phylogenetic tree. GenBank accession number are shown after the clone names. Bootstrap values are indicated at the nodes.

Fig. S8 The core, accessory and unique orthogroups (OGs) in the reconstructed anammox MAGs and published genomes. Core represent that the OGs are found in all genomes, accessory OGs are found in at least two genomes.

Fig. S9 Principal coordinate analysis (PCoA) of the metabolic potential based on the OGs.

Fig. S10 Principal coordinate analysis (PCoA) of the metabolic potential. PCoA performed on the completeness of metabolic pathways in the four enriched anammox bacteria and the reference species (Supplementary Data S5).

Fig. S11 Visualization of gene flow between anammox bacteria and side population.

Fig. S12 Key anammox gene loci diagram among different anammox species. Gene alignments of

the *amt*B (a) and *nar*K (b) loci with flanking genes are shown.

Fig. S13 Phylogenetic analysis of urease subunit gamma protein sequences. Note: The *utp* gene was only annotated in SW510. Bootstrap values are indicated at the nodes.

Fig. S14 Key genes involved in amino acid biosynthesis. Solid and open circles represent the presence/absence of the genes, respectively.

Supplementary Method

Method Reconstructed the Nitrogen Metabolic Network in Different Anammox Consortia.

The reads per million measures were used as estimations of contig abundance in the present study (Maus et al., 2017), which were calculated using Salmon (Patro et al., 2017). Open Reading Frames (ORFs) were predicted for the contigs retrieved from each metagenome using Prodigal (Hyatt et al., 2010). All predicted ORFs were merged and clustered using CD-HIT (V4.8.1) based on sequence identity (90%) and alignment coverage (80%) to obtain non-redundant ORFs (Fu et al., 2012). The nitrogen-cycling profile of each sample was explored by aligning the non-redundant ORFs to a published database NCycDB using BLASTP with an E-value < 10^{-5}. Only those reads with an identity ⩾ 80% and alignment length ⩾ 70% were assigned as corresponding target sequences (Tu et al., 2018). Further, the nitrogen-cycling ORFs were verified against the NCBI-NR database (October 2020 release) using DIAMOND with an E-value < 10^{-5} (Buchfink et al., 2014). The abundances of nitrogen-cycling genes in all samples were obtained by calculating the reads per million measures with Salmon (Patro et al., 2017). To get a snapshot of the overall microbial community in the six samples, taxonomic assignments of all contigs in metagenomic data were conducted according to the script CAT (Cambuy et al., 2016).

Supplementary Texts

Text S1 Microbial Community Structure of The Anammox Consortia. After quality control, sequencing of DNA yielded a total of 720333280 clean reads in the six anammox consortia, and the individual assembly of these reads generated a total of 3118176 contigs (Table S1). The overall microbial community showed that *Proteobacteria*, *Planctomycetes*, *Chloroflexi* and *Bacteroidetes* were the dominant phyla in the anammox sludge with different particle size (Figure S5a). *Nitrosomonas* with low abundance was mainly responsible for nitrification process, and the dominant anammox population *Candidatus* Brocadia showed the highest abundance compared to other anammox bacteria (Figure S5b). In addition, the heterotrophic environment enriched amounts of denitrifying bacteria in the anammox consortia for nitrogen removal, such as *Lautropia*, *Rubrivivax*, *Steroidobacter* and *Thiobacillus*, which were commonly observed in the anammox-based systems (Guo et al., 2021; Podder et al., 2020; Qin et al., 2017; Wang et al., 2019).

Text S2 Nitrogen Metabolic Potential of The Anammox Consortia. Ammonium appears to be mainly removed by anammox and denitrifying bacteria in the plant according to the high abundance of hydrazine synthase genes, nitrate reductase genes, nitrite reductase genes and nitrous-oxide reductase genes (Figure S6a). The abundant cytochrome *c* nitrite reductase genes reflected that the dissimilatory nitrate reduction process (DNRA) may contribute to ammonium production. In addition, the other nitrogen metabolic pathways, including assimilatory nitrate reduction, nitrogen fixation, ammonification, and ammonium assimilation (Figure S6b), also detected in the anammox consortia. Notably, the relative abundance of anammox-related genes accounted for 80% of the detected proteins in the samples (Figure S6c). Following anammox process, denitrification was the second most abundant nitrogen metabolic pathway in the anammox consortia. Moreover,

the large-sized granular sludge (L-1 and L-2) displayed a higher potential capability of anammox than the small-sized (S-1 and S-2), while the anammox metabolic potential in floc sludge displayed the lowest abundance. The abundance of anammox-related genes in SW773 and SW510 were accounted higher than the other known species, which were in line with their abundance (Table S2). In addition, this study evaluated the growth rate of individual anammox members using the iRep algorithm. An iRep value of 1, 1.5 and 2 suggest that 0, 50 and 100% of the cells are replicating, respectively (Brown et al., 2016). As shown in Table S3, the iRep value of SW172 was not available due to its low abundance and low completeness, while anammox species SW773 possessed the highest growth rates in both floc and granular sludge than other anammox species. Taken together, anammox process was primarily contributed to nitrogen removal in these anammox consortia, and the high abundance and replication rates of the two novel anammox species suggested their niche superiority in the full-scale swine wastewater treatment plant.

Table S1 Detailed information of the metagenomes and the obtained contigs.

Sample ID	Clean reads	Contigs number	N50 of contigs
S-1	137337424	585016	3012
S-2	129744243	419882	3352
L-1	132732178	480096	3138
L-2	128090794	488855	2815
F	94635488	583180	2882
A	97793153	561147	2528

Table S2 The relative abundance of four anammox species based on the MetaWRAP.

Sample ID	SW172	SW510	SW745	SW773	Total
S-1	5.32%	12.44%	3.95%	18.26%	39.98%
S-2	0.17%	8.86%	7.51%	24.49%	41.04%
L-1	3.65%	17.79%	2.65%	23.33%	47.42%
L-2	0.21%	3.70%	7.42%	31.91%	43.24%
F	0.10%	12.94%	2.61%	16.75%	32.41%
A	0.51%	18.20%	3.51%	16.09%	38.30%
Average	1.66%	12.32%	4.61%	21.81%	40.40%

Table S3 The replication rates (i.e., the index of replication) of the four anammox species.

Sample ID	SW172	SW510	SW745	SW773
S-1	NA	1.177769552	1.177531086	1.734190524
S-2	NA	1.170482855	1.171012678	1.250779429
L-1	NA	1.159016431	1.18339059	1.307188351
L-2	NA	1.193450818	1.162566295	1.547626578
F	NA	1.200798568	1.23809304	1.394174085
A	NA	1.186657843	1.195720397	1.339429583
Average	NA	1.181362678	1.188052348	1.428898092

Table S4 Reference anammox genomes used for reconstructed anammox genomes functional annotation.

Assembly	Taxonomy	Reference	Assembly	Taxonomy	Reference
GCA_000786775.1	*Ca.* Scalindua brodae	(Speth et al., 2015)	GCA_007618135.1	*Ca.* Brocadia sp. WS118	(Yang et al., 2019)
GCA_000987375.1	*Ca.* Brocadia fulgida	(Ferousi et al., 2013)	GCA_007618155.1	*Ca.* Brocadia sp. BL1	(Yang et al., 2019)
GCA_001567345.1	*Ca.* Brocadia sinica	(Speth et al., 2016)	GCA_007859995.1	*Ca.* Brocadiaceae bacterium S225	(Peeters et al., 2020; Rensink et al., 2020)
GCA_001723765.1	*Ca.* Scalindua rubra	NA	GCA_007860005.1	*Ca.* Brocadiaceae bacterium B188	(Peeters et al., 2020; Rensink et al., 2020)
GCA_002009475.1	*Ca.* Brocadia caroliniensis	(Park et al., 2017)	GCA_008363395.1	*Ca.* Brocadia sp. AMX2	(Zhao et al., 2019)
GCA_002050315.1	*Ca.* Brocadia sp. UTAMX2	(Lawson et al., 2017)	GCA_008363445.1	*Ca.* Jettenia sp. AMX1	(Zhao et al., 2019)
GCA_002050325.1	*Ca.* Brocadia sp. UTAMX1	(Lawson et al., 2017)	GCA_008501815.1	*Ca.* Scalindua sp.	(Ali et al., 2020)
GCA_003577195.1	*Ca.* Brocadia sp.	(Zhao et al., 2018)	GCA_008933285.1	*Ca.* Brocadia sp.	NA
GCA_003577215.1	*Ca.* Brocadia sp.	(Zhao et al., 2018)	GCF_000296795.1	*Ca.* Jettenia caeni	(Hira et al., 2012, p. 1)

GCA_004282735.1	*Ca.* Brocadia sp. BROELEC01	(Shaw et al., 2020)	GCF_000949635.1	*Ca.* Brocadiaceae	(Oshiki et al., 2015)
GCA_004282745.1	*Ca.* Scalindua sp. SCAELEC01	(Shaw et al., 2020)	GCF_001753675.2	*Ca.* Brocadia sapporoensis	(Ali et al., 2016)
GCA_004351875.1	*Ca.* Scalindua sp. AMX11	(Ali et al., 2019)	GCF_002443295.1	*Ca.* Scalindua sp. husup-a2	(Oshiki et al., 2017)
GCA_005524015.1	*Ca.* Jettenia ecosi	(Mardanov et al., 2019)	GCF_900232105.1	*Ca.* Brocadiaceae	(Frank et al., 2018)

Table S5 Key functional genes involved in central carbon metabolism, including Carbon fixation (Wood-Ljungdahl pathway), Gluconeogenesis (Glycolysis pathway), Pentose phosphate pathway, Glycogen metabolism and TCA cycle.

KO	Abbreviation	Name
K00123	fdhA	Formate dehydrogenase major subunit
K01938	fhs	Formate-tetrahydrofolate ligase
K01491	folD	Methylenetetrahydrofolate dehydrogenase (NADP+)/methenyltetrahydrofolate cyclohydrolase
K00548	metH	5-methyltetrahydrofolate/Methyltransferase
K00194	cdhD/cooS	Acetyl-CoA decarbonylase/synthase, CODH/ACS complex delta
K00197	cdhE/cooS	Acetyl-CoA decarbonylase/synthase, CODH/ACS complex gamma
K00198	cooS	CO dehydrogenase catalytic subunit
K07321	cooS	CO dehydrogenase maturation factor
K00193	cdhC	CO-methylating acetyl-CoA synthase
K01895	ACS	Acetyl-CoA synthetase
K01905	ACS	Acetyl-CoA synthetase
K00925	ackA	Acetate kinase
K00170	porB	Pyruvate ferredoxin oxidoreductase beta subunit
K00169	porA	Pyruvate ferredoxin oxidoreductase alpha subunit
K00171	porD	Pyruvate ferredoxin oxidoreductase delta subunit
K00172	porC	Pyruvate ferredoxin oxidoreductase gamma subunit
K01006	ppdk	Pyruvate, orthophosphate dikinase
K01689	ENO	Enolase/phosphopyruvate hydratase
K15635	PGAM	2,3-bisphosphoglycerate-independent phosphoglycerate mutase
K00927	PGK	Phosphoglycerate kinase
K00134	GAPDH	Glyceraldehyde 3-phosphate dehydrogenase
K01624	FBA	Fructose-1,6-bisphosphate aldolase, class II
K08321	FBA	Fructose-1,6-biphosphate aldolase class I
K00850	pfkA	6-phosphofructo kinase 1
K03841	FBP	Fructose-1,6-bisphosphatase I
K01810	GPI	Glucose-6-phosphate isomerase
K00036	G6PD	Glucose-6-phosphate 1-dehydrogenase
K01057	6PGL	6-phosphogluconolactonase
K00033	PGD	6-phosphogluconate dehydrogenase
K01783	RPE	Ribulose-5-phosphate 3-epimerase
K01808	RPI	Ribose-5-phosphate isomerase
K00615	TKT	Transketolase
K00616	TAL	Transaldolase

K01835	Pgm	Phosphoglucomutase
K00703	GlgA	Glycogen synthase
K00975	GlgC	G-1P adenylyltransferase
K00700	GlgB	α-1,4-glucan branching enzyme
K00688	GlgP	Glycogen phosphorylase
K02438	GlgX	Glycogen operon protein
K06044	TreY	Malto-oligosyltrehalose synthase
K01236	TreZ	Maltooligosyltrehalose trehalohydrolase
K13057	TreT	Trehalose synthase
NA	cs	Citrate synthase
K01681	aco	Aconitate hydratase
K00031	idh	Isocitrate dehydrogenase
K00174	korA	2-ketoglutarate/2-oxoacid ferredoxin oxidoreductase subunit alpha
K00175	korB	2-ketoglutarate/2-oxoacid ferredoxin oxidoreductase subunit beta
K01958	pyc	Pyruvate carboxylase
K00024	mdh	Malate dehydrogenase NAD dependent
K01677	fh	Fumarate hydratase subunit alpha
K00239	frdA	Succinate dehydrogenase/fumarate reductase, flavoprotein subunit
K00240	frdB	Succinate dehydrogenase cytochrome b-556 subunit C
K01903	sucC	Succinyl-CoA synthetase beta subunit
K01904	sucD	Succinyl-CoA synthetase alpha subunit

Table S6 Key genes involved in methionine biosynthesis (i.e., the KEGG module M00017).

KO	Abbreviation	Name	Copies			
			SW172	SW510	SW745	SW773
K00928	lysC	aspartate kinase	1	1	1	1
K12524	thrA	bifunctional aspartokinase/homoserine dehydrogenase 1	0	0	0	0
K12525	metL	bifunctional aspartokinase/homoserine dehydrogenase 2	0	0	0	0
K00133	asd	aspartate-semialdehyde dehydrogenase	1	1	1	1
K00003	hom	homoserine dehydrogenase	1	1	1	1
K00651	metA	homoserine O-succinyltransferase/O-acetyltransferase	0	0	0	0
K00641	metX	homoserine O-acetyltransferase/O-succinyltransferase	0	0	0	0
K01739	metB	cystathionine gamma-synthase	0	0	0	0
K01760	metC	cysteine-S-conjugate beta-lyase	0	0	0	0
K14155	patB	cysteine-S-conjugate beta-lyase	0	0	0	0
K00548	metH	5-methyltetrahydrofolate--homocysteine methyltransferase	0	0	0	0
K24042	yitJ	methionine synthase/methylenetetrahydrofolate reductase (NADPH)	0	0	0	0
K00549	metE	5-methyltetrahydropteroyltriglutamate--homocysteine methyltransferase	3	1	3	3

Table S7 Key genes involved in pantothenate biosynthesis (i.e., the KEGG module M00119).

KO	Abbreviation	Name	Copies			
			SW172	SW510	SW745	SW773
K00826	ilvE	branched-chain amino acid aminotransferase	3	1	2	2
K00606	panB	3-methyl-2-oxobutanoate hydroxymethyltransferase	0	0	0	0
K00077	panE	2-dehydropantoate 2-reductase	0	0	0	0
K01579	panD	aspartate 1-decarboxylase	2	1	1	1
K01918	panC	pantoate--beta-alanine ligase	1	1	1	0
K13799	panC-cmk	pantoate ligase/CMP/dCMP kinase	1	1	1	0

Table S8 Key genes involved in folate biosynthesis, including three KEGG modules M00126, M00840 and M00841.

KO	Abbreviation	Name	Copies			
			SW172	SW510	SW745	SW773
K00287	DHFR/folA	dihydrofolate reductase	1	0	0	0
K00796	folP	dihydropteroate synthase	1	1	1	1
K00950	folK	2-amino-4-hydroxy-6-hydroxymethyldihydropteridine diphosphokinase	1	1	1	1
K01077	phoA/B	alkaline phosphatase	0	0	0	2
K01113	phoD	alkaline phosphatase D	0	0	0	0
K01495	GCH1	GTP cyclohydrolase IA	1	0	2	0
K01633	folB	7,8-dihydroneopterin aldolase/epimerase/oxygenase	0	0	1	0
K08310	nudB	dihydroneopterin triphosphate diphosphatase	0	0	0	0
K09007	folE2	GTP cyclohydrolase IB	0	0	0	0
K11754	folC	dihydrofolate synthase/folylpolyglutamate synthase	1	1	1	1
K14652	ribBA	3,4-dihydroxy 2-butanone 4-phosphate synthase/GTP cyclohydrolase II	0	0	0	0
K19965	folQ	dihydroneopterin triphosphate pyrophosphohydrolase	0	0	0	0
K20457	DHFS	dihydrofolate synthase	0	0	0	0
K22099	folC2	dihydrofolate synthase/folylpolyglutamate synthase	0	0	0	0
K22101	PTPS	dihydroneopterin triphosphate aldolase (PTPS-III)/6-pyruvoyltetrahydropterin synthase	0	0	0	0

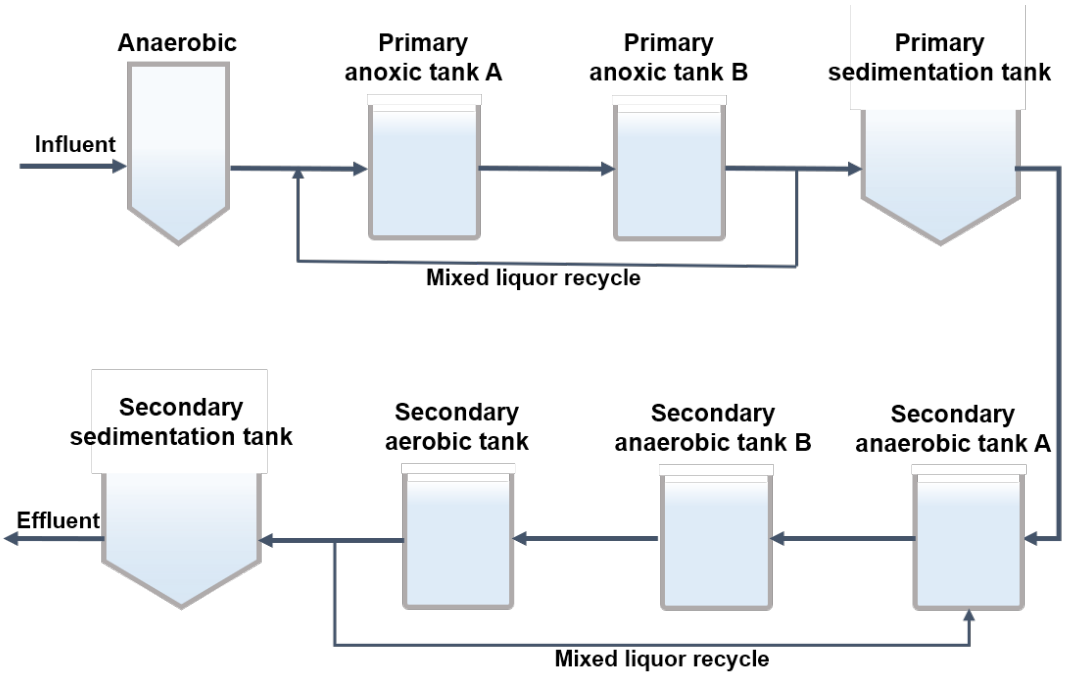

Fig. S1 Schematic diagram of biological treatment process in the full-scale swine wastewater treatment plant.

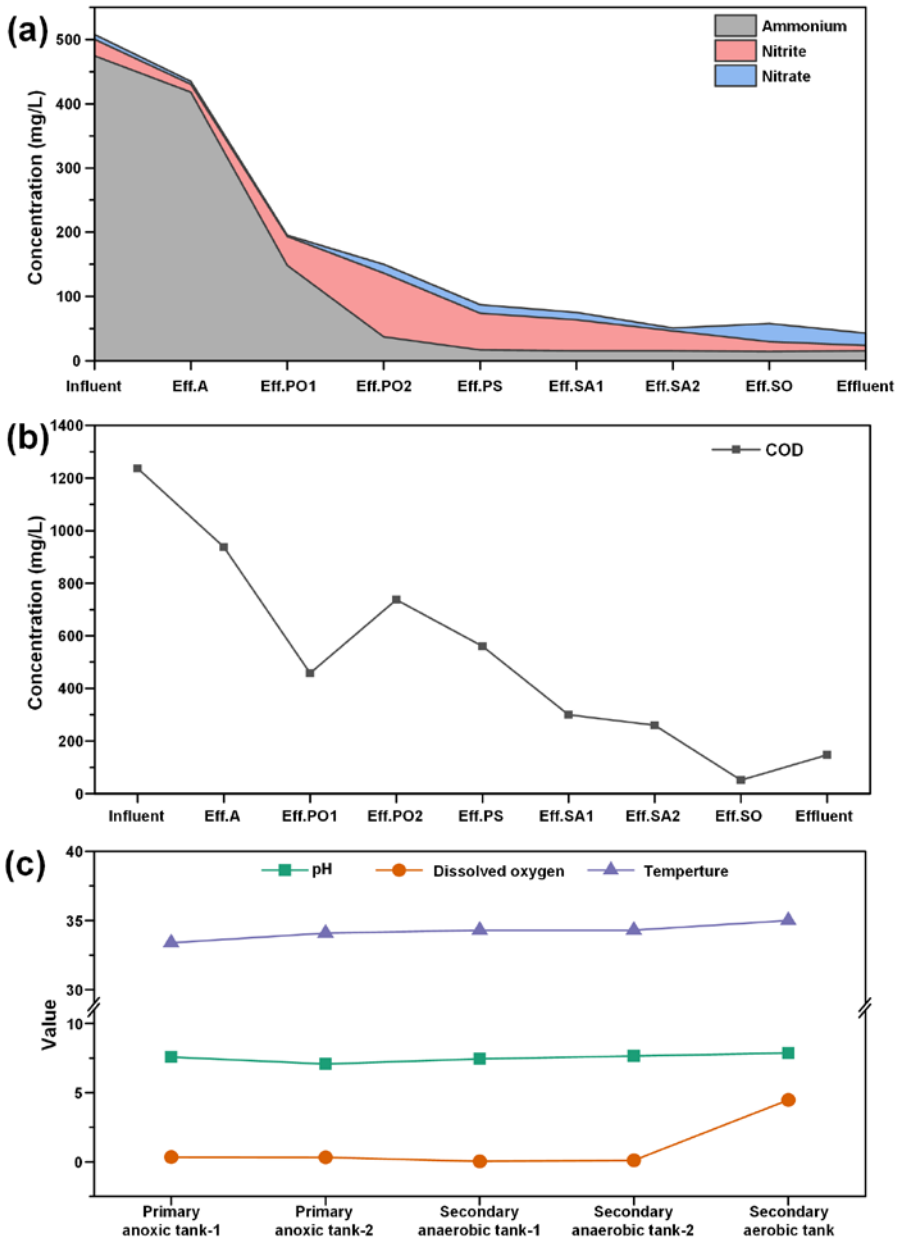

Fig. S2 Concentrations of nitrogen (a) and organic matter (b) and the pH, dissolved oxygen, and temperature (c) in different tanks of the full-scale swine wastewater treatment plant. Eff.A: effluent of the anaerobic process; Eff.PO1: effluent of the primary anoxic tank-1; Eff.PO2: effluent of the primary anoxic tank-2; Eff.PS: effluent of the primary sedimentation; Eff. SA1: effluent of the secondary anaerobic tank-1; Eff. SA2: effluent of the secondary anaerobic tank-2; Eff.SO: effluent of the secondary aerobic tank.

Fig. S3 Photos of the floc and granular sludge.

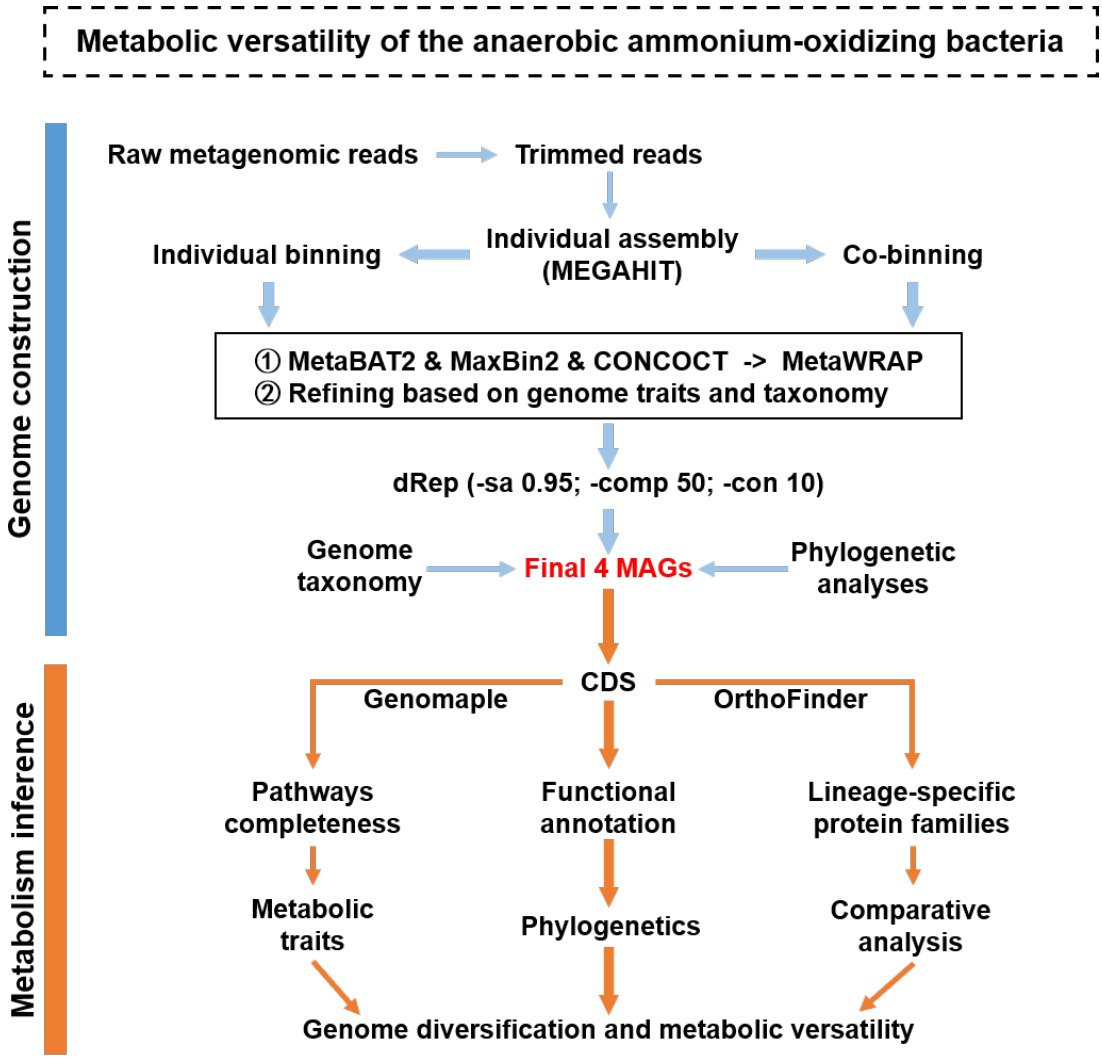

Fig. S4 The analysis pipeline for metabolic versatility in this study, including (1) the approaches to reconstruct genome bins, (2) the approaches to infer metabolisms of genomes.

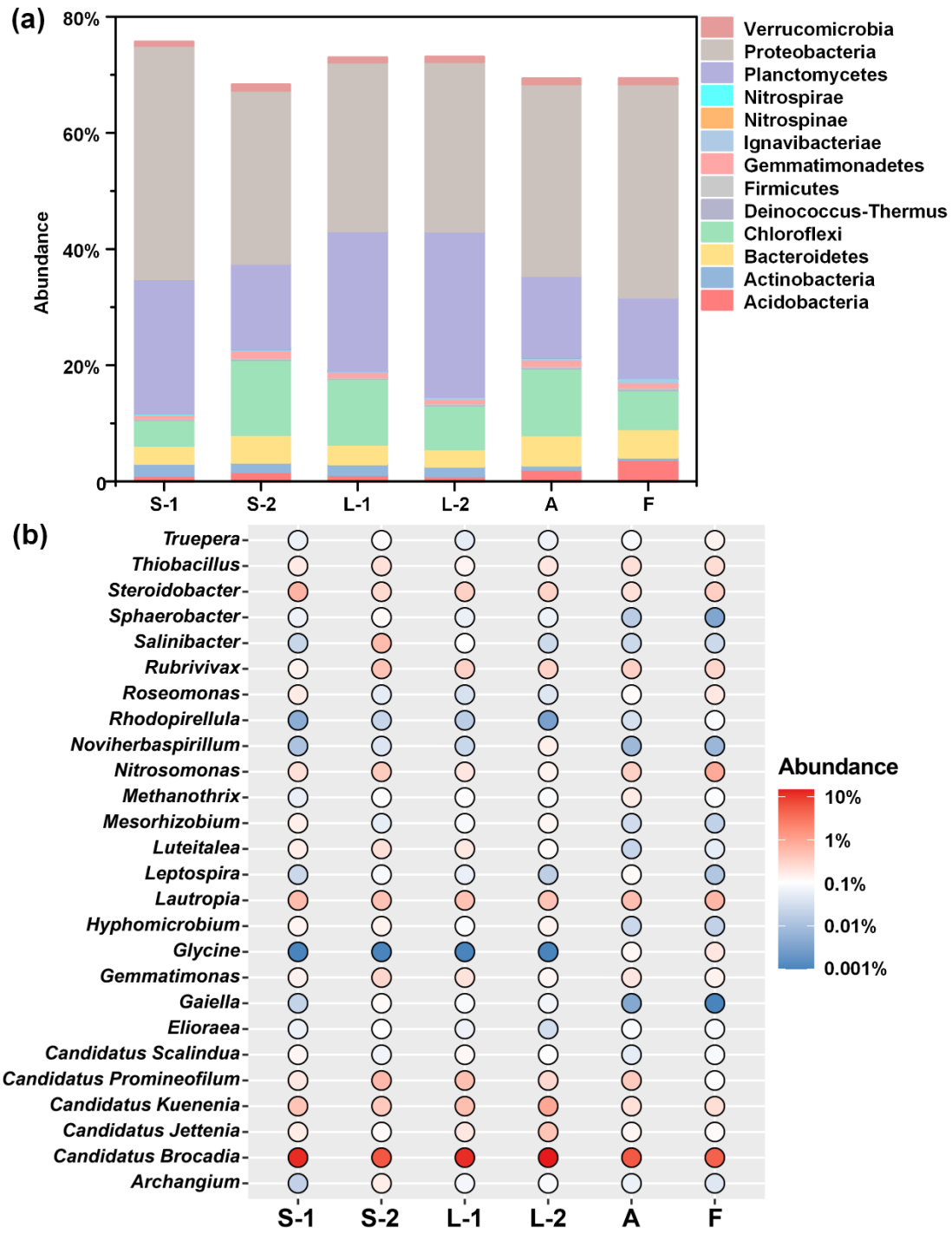

Fig. S5 Microbial community composition of the major phyla (a) and genus (b) in the anammox consortia according to the contig analysis.

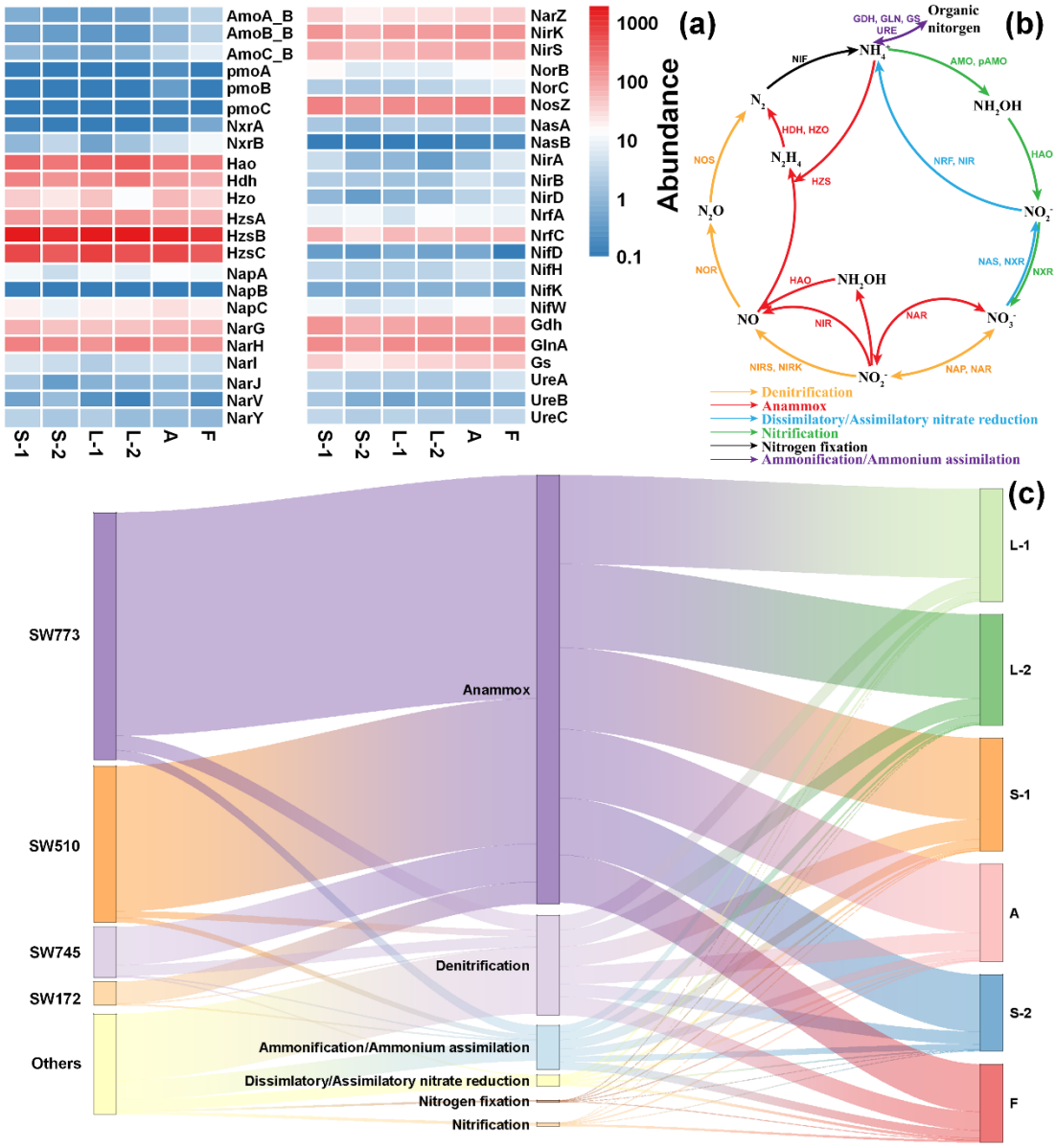

Fig. S6 (a) Total abundance of nitrogen metabolic genes. (b) Reconstructed nitrogen metabolic network. (c) Total abundance of nitrogen metabolic processes in different anammox consortia and microorganisms. The abundance of genes was calculated based on the Salmon, and the total abundance of all genes reached 1000000.

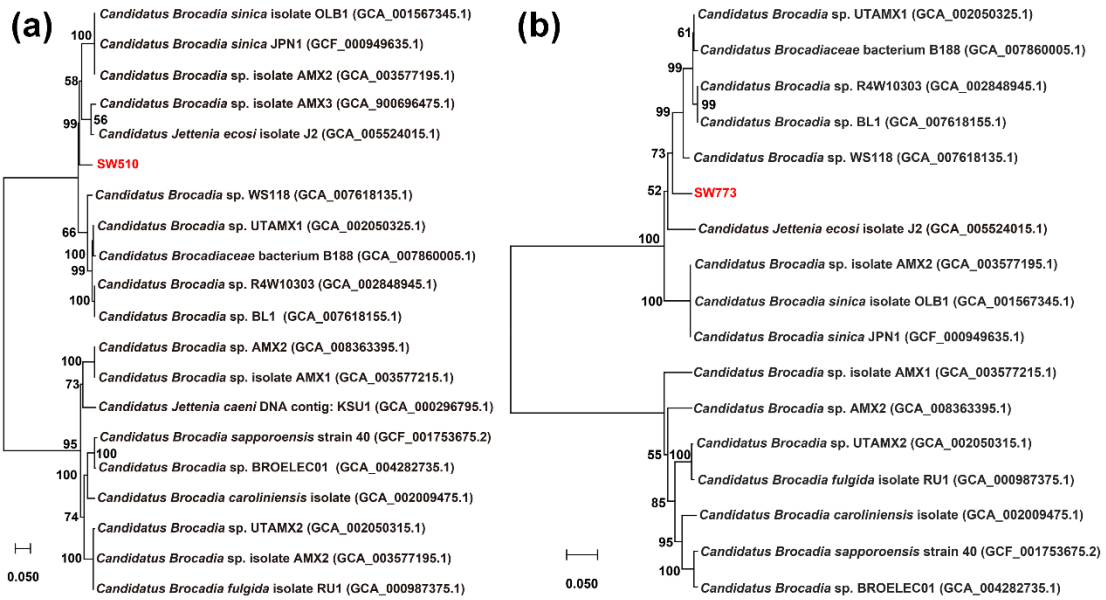

Fig. S7 Position SW510 (a) and SW773 (b) on neighbor-joining 16S rRNA gene phylogenetic tree. GenBank accession number are shown after the clone names. Bootstrap values are indicated at the nodes.

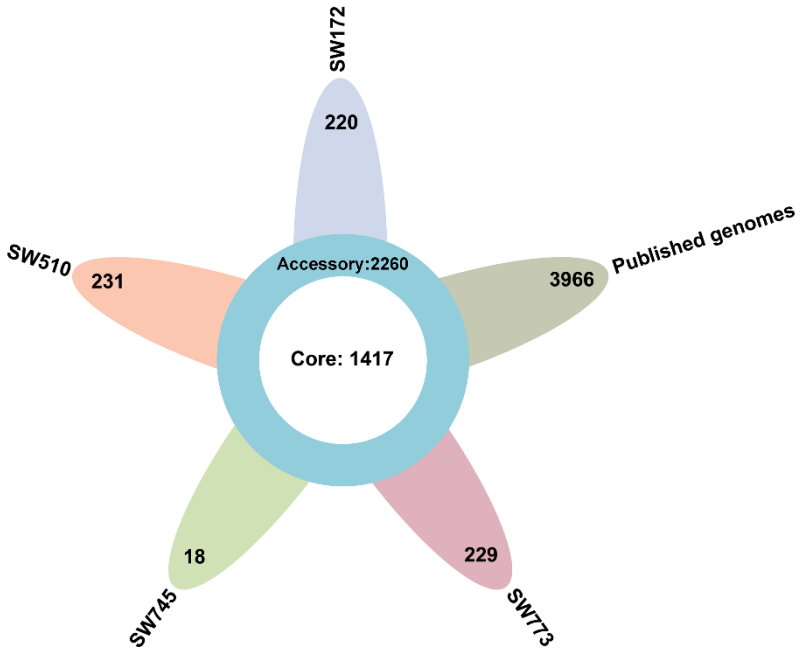

Fig. S8 The core, accessory and unique orthogroups (OGs) in the reconstructed anammox MAGs and published genomes. Core represent that the OGs are found in all genomes, accessory OGs are found in at least two genomes.

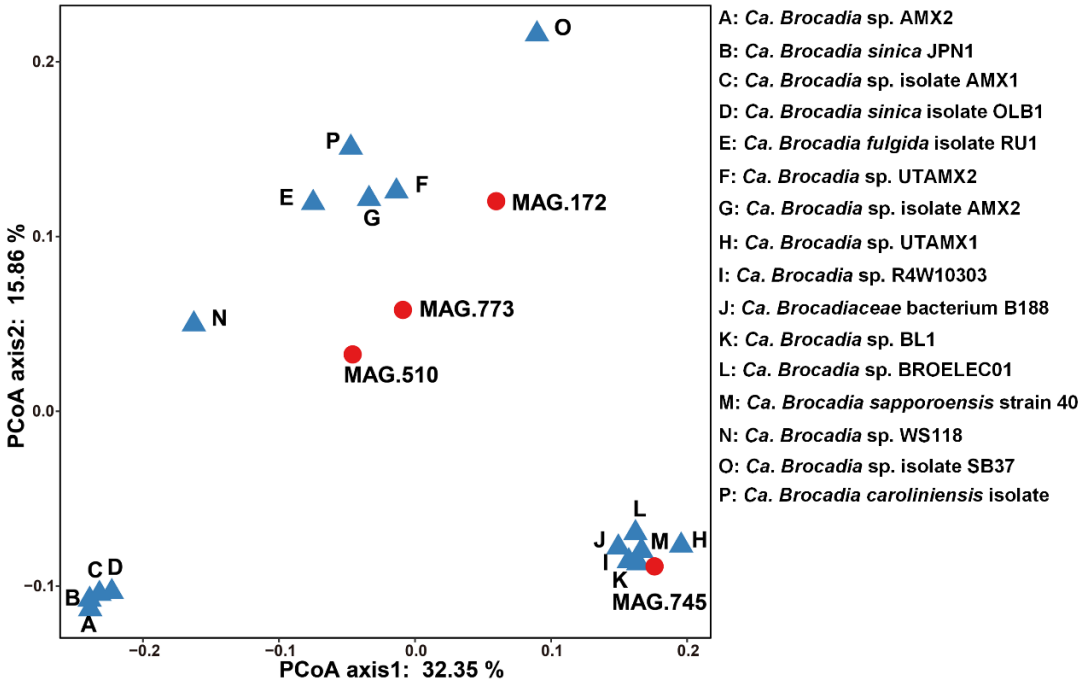

Fig. S9 Principal coordinate analysis (PCoA) of the metabolic potential based on the OGs.

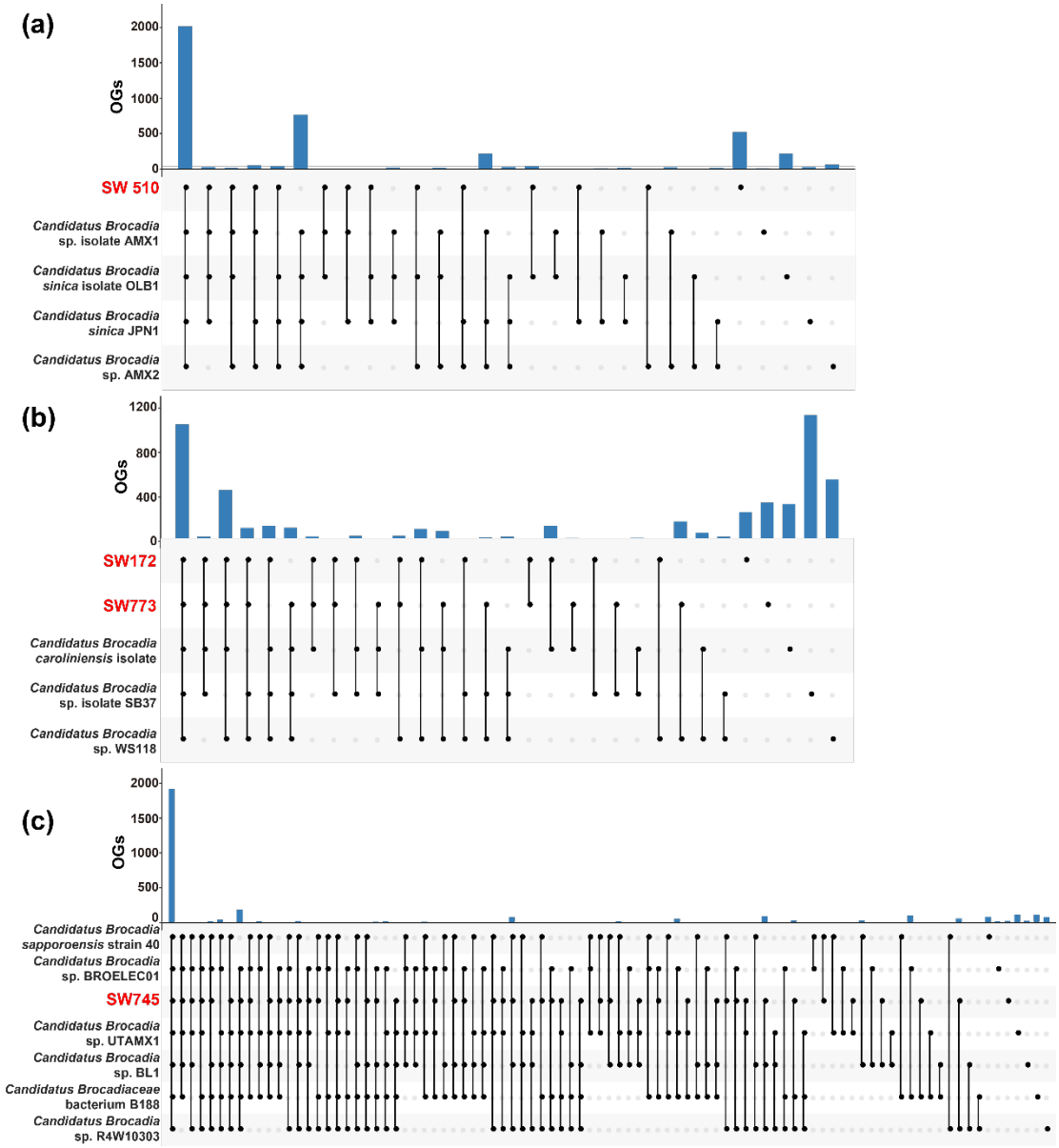

Fig. S10 The shared and unique orthogroups (OGs) among these species with low phylogenetic distance.

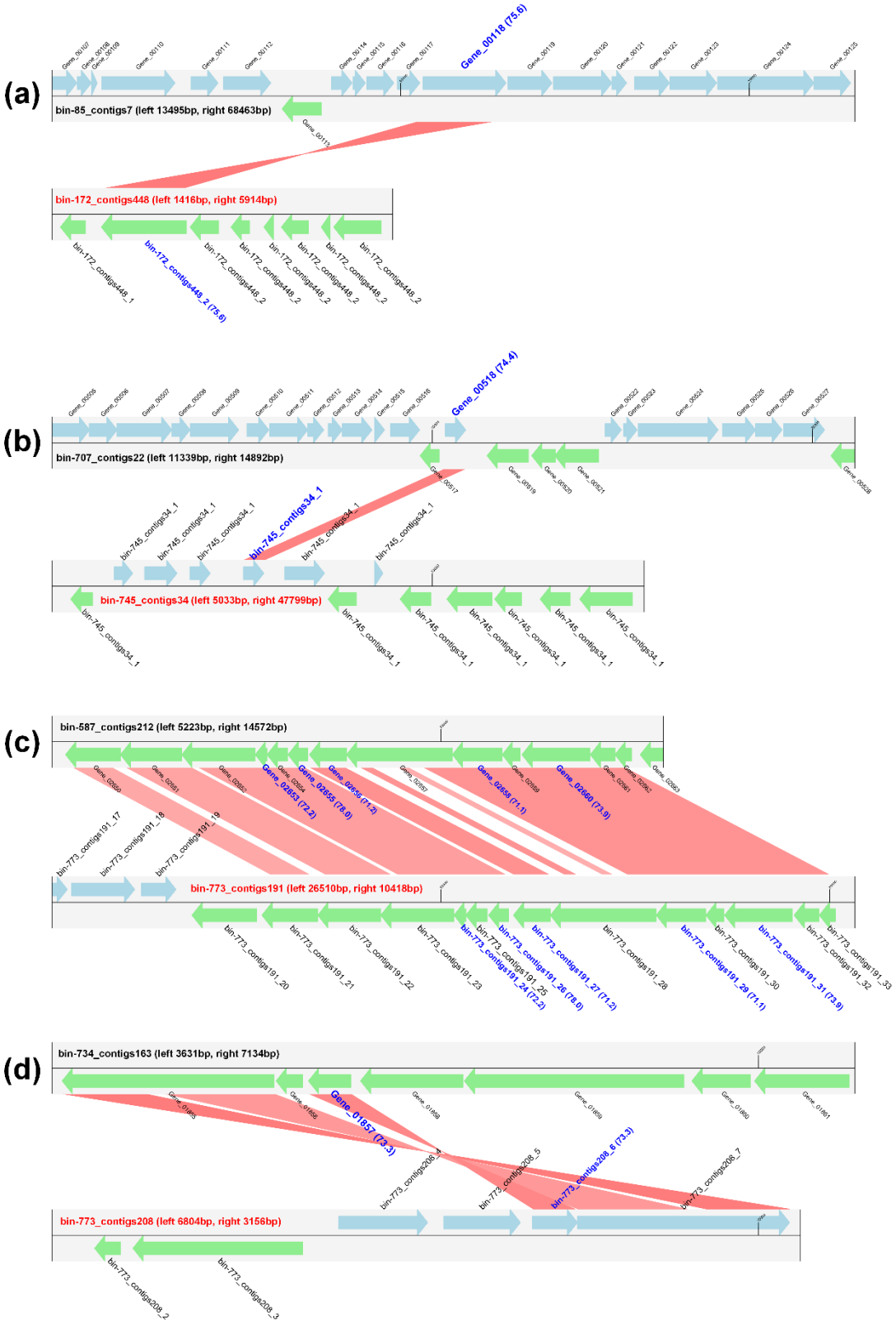

Fig. S11 Visualization of gene flow between anammox bacteria and side population.

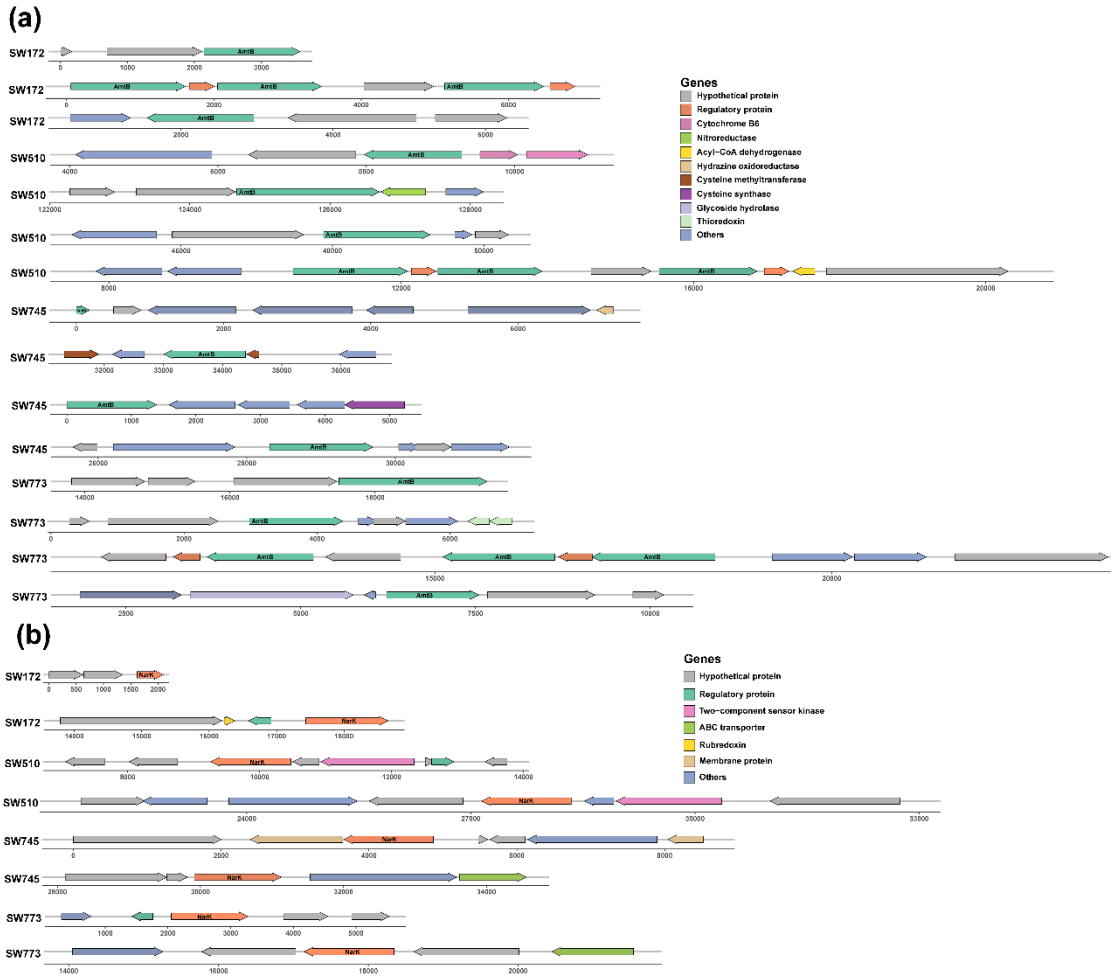

Fig. S12 Key anammox gene loci diagram among different anammox species. Gene alignments of the *amt*B (a) and *nar*K (b) loci with flanking genes are shown. Color represents the homologous genes, and the genes without functional information are identified as hypothetical protein. Genes and noncoding regions are drawn to scale. The right and left arrows represent the orientation (1) and (-1), respectively.

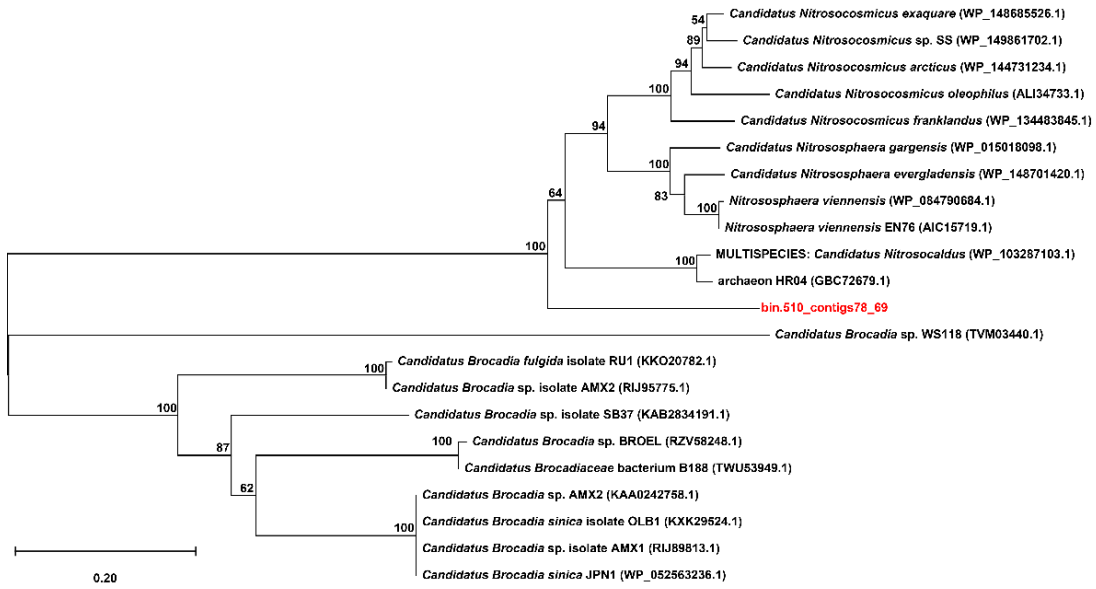

Fig. S13 Phylogenetic analysis of urease subunit gamma protein sequences. Note: The *utp* gene was only annotated in SW510. Bootstrap values are indicated at the nodes.

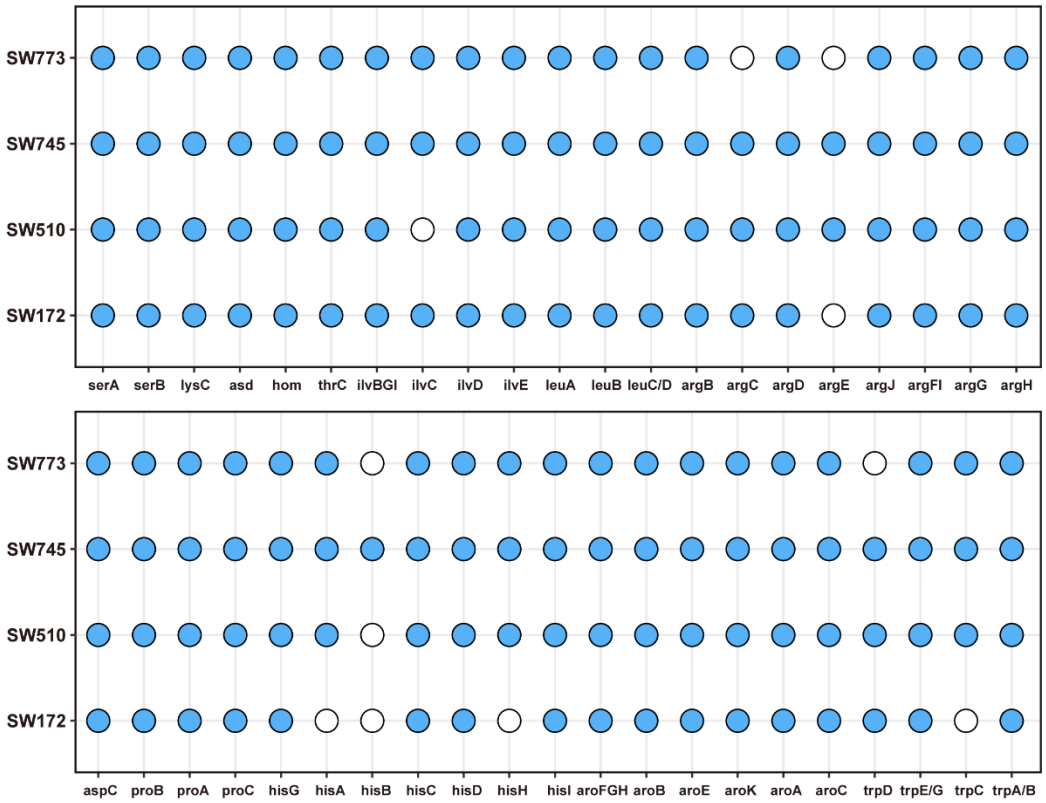

Fig. S14 Key genes involved in amino acid biosynthesis. Solid and open circles represent the presence/absence of the genes, respectively.

References

Ali, M., Haroon, M.F., Narita, Y., Zhang, L., Shaw, D.R., Okabe, S., Saikaly, P.E., 2016. Draft Genome Sequence of the Anaerobic Ammonium-Oxidizing Bacterium "Candidatus Brocadia sp. 40." Genome Announc. 4. https://doi.org/10.1128/genomeA.01377-16

Ali, M., Shaw, D.R., Saikaly, P.E., 2020. Application of an enrichment culture of the marine anammox bacterium "Ca. Scalindua sp. AMX11" for nitrogen removal under moderate salinity and in the presence of organic carbon. Water Res. 170, 115345. https://doi.org/10.1016/j.watres.2019.115345

Ali, M., Shaw, D.R., Saikaly, P.E., 2019. Draft Genome Sequence of a Novel Marine Anaerobic Ammonium-Oxidizing Bacterium, "Candidatus Scalindua sp." Microbiol. Resour. Announc. 8. https://doi.org/10.1128/MRA.00297-19

Brown, C.T., Olm, M.R., Thomas, B.C., Banfield, J.F., 2016. Measurement of bacterial replication rates in microbial communities. Nat. Biotechnol. 34, 1256–1263. https://doi.org/10.1038/nbt.3704

Buchfink, B., Xie, C., Huson, D.H., 2014. Fast and sensitive protein alignment using DIAMOND. Nat. Methods 12, 59.

Cambuy, D.D., Coutinho, F.H., Dutilh, B.E., 2016. Contig annotation tool CAT robustly classifies assembled metagenomic contigs and long sequences. bioRxiv 072868. https://doi.org/10.1101/072868

Ferousi, C., Speth, D.R., Reimann, J., Op den Camp, H.J., Allen, J.W., Keltjens, J.T., Jetten, M.S., 2013. Identification of the type II cytochrome cmaturation pathway in anammox bacteria by comparative genomics. BMC Microbiol. 13, 265. https://doi.org/10.1186/1471-2180-13-265

Frank, J., Lücker, S., Vossen, R.H.A.M., Jetten, M.S.M., Hall, R.J., Op den Camp, H.J.M., Anvar, S.Y., 2018. Resolving the complete genome of Kuenenia stuttgartiensis from a membrane bioreactor enrichment using Single-Molecule Real-Time sequencing. Sci. Rep. 8, 4580. https://doi.org/10.1038/s41598-018-23053-7

Fu, L., Niu, B., Zhu, Z., Wu, S., Li, W., 2012. CD-HIT: accelerated for clustering the next-generation sequencing data. Bioinformatics 28, 3150–3152. https://doi.org/10.1093/bioinformatics/bts565

Guo, Y., Zhao, Y., Tang, X., Na, T., Pan, J., Zhao, H., Liu, S., 2021. Deciphering bacterial social traits via diffusible signal factor (DSF) -mediated public goods in an anammox community. Water Res. 191, 116802. https://doi.org/10.1016/j.watres.2020.116802

Hira, D., Toh, H., Migita, C.T., Okubo, H., Nishiyama, T., Hattori, M., Furukawa, K., Fujii, T., 2012. Anammox organism KSU-1 expresses a NirK-type copper-containing nitrite reductase instead of a NirS-type with cytochrome cd 1. FEBS Lett. 586, 1658–1663. https://doi.org/10.1016/j.febslet.2012.04.041

Hyatt, D., Chen, G.-L., LoCascio, P.F., Land, M.L., Larimer, F.W., Hauser, L.J., 2010. Prodigal: prokaryotic gene recognition and translation initiation site identification. BMC Bioinformatics 11, 119. https://doi.org/10.1186/1471-2105-11-119

Lawson, C.E., Wu, S., Bhattacharjee, A.S., Hamilton, J.J., McMahon, K.D., Goel, R., Noguera, D.R., 2017. Metabolic network analysis reveals microbial community interactions in anammox granules. Nat. Commun. 8, 1–12. https://doi.org/10.1038/ncomms15416

Mardanov, A.V., Beletsky, A.V., Ravin, N.V., Botchkova, E.A., Litti, Y.V., Nozhevnikova, A.N., 2019. Genome of a novel bacterium "Candidatus Jettenia ecosi" reconstructed from the metagenome of an anammox bioreactor. Front. Microbiol. 10, 2442. https://doi.org/10.3389/fmicb.2019.02442

Maus, I., Bremges, A., Stolze, Y., Hahnke, S., Cibis, K.G., Koeck, D.E., Kim, Y.S., Kreubel, J., Hassa, J., Wibberg,

D., Weimann, A., Off, S., Stantscheff, R., Zverlov, V.V., Schwarz, W.H., König, H., Liebl, W., Scherer, P., McHardy, A.C., Sczyrba, A., Klocke, M., Pühler, A., Schlüter, A., 2017. Genomics and prevalence of bacterial and archaeal isolates from biogas-producing microbiomes. Biotechnol. Biofuels 10, 264. https://doi.org/10.1186/s13068-017-0947-1

Oshiki, M., Mizuto, K., Kimura, Z., Kindaichi, T., Satoh, H., Okabe, S., 2017. Genetic diversity of marine anaerobic ammonium-oxidizing bacteria as revealed by genomic and proteomic analyses of 'Candidatus Scalindua japonica.' Environ. Microbiol. Rep. 9, 550–561. https://doi.org/10.1111/1758-2229.12586

Oshiki, M., Shinyako-Hata, K., Satoh, H., Okabe, S., 2015. Draft Genome Sequence of an Anaerobic Ammonium-Oxidizing Bacterium, "Candidatus Brocadia sinica." Genome Announc. 3. https://doi.org/10.1128/genomeA.00267-15

Park, H., Brotto, A.C., van Loosdrecht, M.C.M., Chandran, K., 2017. Discovery and metagenomic analysis of an anammox bacterial enrichment related to Candidatus "Brocadia caroliniensis" in a full-scale glycerol-fed nitritation-denitritation separate centrate treatment process. Water Res. 111, 265–273. https://doi.org/10.1016/j.watres.2017.01.011

Patro, R., Duggal, G., Love, M.I., Irizarry, R.A., Kingsford, C., 2017. Salmon provides fast and bias-aware quantification of transcript expression. Nat. Methods 14, 417–419. https://doi.org/10.1038/nmeth.4197

Peeters, S.H., Wiegand, S., Kallscheuer, N., Jogler, M., Heuer, A., Jetten, M.S.M., Rast, P., Boedeker, C., Rohde, M., Jogler, C., 2020. Three marine strains constitute the novel genus and species Crateriforma conspicua in the phylum Planctomycetes. Antonie Van Leeuwenhoek 113, 1797–1809. https://doi.org/10.1007/s10482-019-01375-4

Podder, A., Reinhart, D., Goel, R., 2020. Nitrogen management in landfill leachate using single-stage anammox process-illustrating key nitrogen pathways under an ecogenomics framework. Bioresour. Technol. 312, 123578. https://doi.org/10.1016/j.biortech.2020.123578

Qin, Y., Cao, Y., Ren, J., Wang, T., Han, B., 2017. Effect of glucose on nitrogen removal and microbial community in anammox-denitrification system. Bioresour. Technol. 244, 33–39. https://doi.org/10.1016/j.biortech.2017.07.124

Rensink, S., Wiegand, S., Kallscheuer, N., Rast, P., Peeters, S.H., Heuer, A., Boedeker, C., Jetten, M.S.M., Rohde, M., Jogler, M., Jogler, C., 2020. Description of the novel planctomycetal genus Bremerella, containing Bremerella volcania sp. nov., isolated from an active volcanic site, and reclassification of Blastopirellula cremea as Bremerella cremea comb. nov. Antonie Van Leeuwenhoek 113, 1823–1837. https://doi.org/10.1007/s10482-019-01378-1

Shaw, D.R., Ali, M., Katuri, K.P., Gralnick, J.A., Reimann, J., Mesman, R., van Niftrik, L., Jetten, M.S.M., Saikaly, P.E., 2020. Extracellular electron transfer-dependent anaerobic oxidation of ammonium by anammox bacteria. Nat. Commun. 11, 2058. https://doi.org/10.1038/s41467-020-16016-y

Speth, D.R., in 't Zandt, M.H., Guerrero-Cruz, S., Dutilh, B.E., Jetten, M.S.M., 2016. Genome-based microbial ecology of anammox granules in a full-scale wastewater treatment system. Nat. Commun. 7, 11172. https://doi.org/10.1038/ncomms11172

Speth, D.R., Russ, L., Kartal, B., Camp, H.J.M. op den, Dutilh, B.E., Jetten, M.S.M., 2015. Draft Genome Sequence of Anammox Bacterium "Candidatus Scalindua brodae," Obtained Using Differential Coverage Binning of Sequencing Data from Two Reactor Enrichments. Genome Announc. 3. https://doi.org/10.1128/genomeA.01415-14

Tu, Q., Lin, L., Cheng, L., Deng, Y., He, Z., 2018. NCycDB: a curated integrative database for fast and accurate metagenomic profiling of nitrogen cycling genes. Bioinformatics 35, 1040–1048. https://doi.org/10.1093/bioinformatics/bty741

Wang, D., Li, T., Huang, K., He, X., Zhang, X.-X., 2019. Roles and correlations of functional bacteria and genes in the start-up of simultaneous anammox and denitrification system for enhanced nitrogen removal. Sci. Total Environ. 655, 1355–1363. https://doi.org/10.1016/j.scitotenv.2018.11.321

Yang, Y., Pan, J., Zhou, Z., Wu, J., Liu, Y., Lin, J.-G., Hong, Y., Li, X., Li, M., Gu, J.-D., 2019. Complex microbial nitrogen-cycling networks in three distinct anammox-inoculated wastewater treatment systems. Water Res. 168, 115142. https://doi.org/10.1016/j.watres.2019.115142

Zhao, Y., Feng, Y., Chen, L., Niu, Z., Liu, S., 2019. Genome-centered omics insight into the competition and niche differentiation of Ca. Jettenia and Ca. Brocadia affiliated to anammox bacteria. Appl. Microbiol. Biotechnol. 103, 8191–8202. https://doi.org/10.1007/s00253-019-10040-9

Zhao, Y., Liu, Shufeng, Jiang, B., Feng, Y., Zhu, T., Tao, H., Tang, X., Liu, Sitong, 2018. Genome-centered metagenomics analysis reveals the symbiotic organisms possessing ability to cross-feed with anammox bacteria in anammox consortia. Environ. Sci. Technol. 52, 11285–11296. https://doi.org/10.1021/acs.est.8b02599